RSC Advances

PAPER

View Article Online
View Journal | View Issue

Cite this: *RSC Adv.*, 2017, **7**, 50166

Electrostatically driven scalable synthesis of MoS_2–graphene hybrid films assisted by hydrophobins†

Jasneet Kaur, *[ab] Alessandro Vergara,[cde] Manuela Rossi,[f] Alfredo Maria Gravagnuolo,[cg] Mohammadhassan Valadan,[a] Federica Corrado,[h] Mariarosaria Conte,[i] Felice Gesuele,[a] Paola Giardina[c] and Carlo Altucci*[a]

Liquid processing of 2D crystals offers scalable strategies for the production of 2D materials. Herein, we produce the hybrids of MoS_2/graphene, consisting of few-layered nanosheets of luminescent MoS_2 and biofunctionalized few-layered graphene assisted by the Vmh2 hydrophobin, a self-assembling adhesive fungal protein, through a green route of production. The functionalization of the graphene flakes assisted by Vmh2 adds surface charge, which enables electrostatic interaction between MoS_2 and graphene flakes, leading to the van der Waals coupling. The surface morphology of 2D material based films is analyzed through optical imaging, scanning and transmission electron microscopy. The produced dispersions of MoS_2, bGr and the hybrid solutions, are investigated by electrophoretic mobility, UV-Vis, Raman and photoluminescence spectroscopy. Interestingly, the effect of van der Waals interactions between the layers of MoS_2 and bGr crystals are evidenced through the significant upshift of 14 cm^{-1} in the G′ Raman peak of graphene and an upshift of 1.4 cm^{-1} of the A_{1g} peak of MoS_2. Due to the formation of heterostructures, significant quenching of the characteristic photoluminescence emitted from the monolayers of MoS_2 was also observed, indicating the charge transfer process occurring between the crystal layers. This approach of scalable synthesis of 2D material based nano-bio hybrids offers economic and eco-friendly solutions to promote novel applications in biosensing and photodetection.

Received 5th September 2017
Accepted 19th October 2017

DOI: 10.1039/c7ra09878b

rsc.li/rsc-advances

Introduction

The rising interest in two-dimensional (2D) materials, beyond graphene, is to unveil the potential of 2D alternatives and to supplement the gapless feature of graphene, with interesting electronic properties from other analogues such as semiconducting transition metal dichalcogenides (TMDs) and insulating hexagonal boron nitride (hBN).[1,2] These novel 2D TMD crystals offer promising applications due to their unique physicochemical features, including a broad absorption spectrum, ultra-thin sheet structures, mechanical flexibility and high optical absorption.[3–5] Moreover, since graphene exhibits remarkable electrical and thermal conductivities, optical transparency, elasticity and strength, crucial for flexible electronics, thus research efforts have been dedicated to integrate distinct 2D materials to produce van der Waals heterostructures (vdW), which could offer novel and tailored optoelectronic features with varying functionalities.[6–8] Among TMDs, few-layered MoS_2 is an interesting candidate with unique properties for a range of electronics and biomedical applications, which can also complement with graphene, since it combines the excellent optical properties of MoS_2 with the high mobility and transparency of graphene.[9,10] Therefore, the possible heterostructure of MoS_2/graphene would form a perfect couple, which can offer novel applications in nanoelectronics and optoelectronics, due to the superlative properties of semiconductor/(semi) metal heterojunction contact.[11,12]

In order to exploit the intriguing properties of vdW heterostructures, the immediate requirement is to develop scalable production route for the exfoliation of high-quality 2D materials through eco-friendly and low-cost techniques. In contrast to conventional epitaxially grown routes for heterostructures, involving micromechanical cleavage followed by critical transfer process, and chemical vapor deposition, the solution

[a]Department of Physics "Ettore Pancini", University of Naples Federico II, Naples, Italy. E-mail: jasneet@fisica.unina.it; carlo.altucci@unina.it
[b]Akal College of Basic Sciences, Eternal University, Baru Sahib, Himachal Pradesh, India. E-mail: jasneet.physics@gmail.com
[c]Department of Chemical Sciences, University of Naples Federico II, Naples, Italy
[d]CEINGE Biotecnologie Avanzate scarl, Naples, Italy
[e]Institute of Biostructures and Bioimaging, CNR, Naples, Italy
[f]Department of Earth, Environment and Resources Sciences, University of Naples Federico II, Naples, Italy
[g]Division of Pharmacy and Optometry, Faculty of Biology, Medicine and Health, The University of Manchester, UK
[h]Istituto Zooprofilattico Sperimentale del Mezzogiorno, Portici, Italy
[i]IRCCS, SDN, Via E. Gianturco 113, 80143, Naples, Italy

† Electronic supplementary information (ESI) available. See DOI: 10.1039/c7ra09878b

processing technique with liquid-phase exfoliation (LPE) offers advantages for scalability and cost-reduction with production of high-quality, few-layered 2D materials based dispersions.[13,14] These water-based dispersions consist of 2D nanosheets which can be deposited on the substrates through drop-casting or spin-coating methods.[15,16] However, in several literature reports, 2D materials based dispersions are produced by exfoliation of bulk crystals in the presence of toxic organic solvents,[17,18] which need to be replaced by eco-friendly and biocompatible solvents for environmental and health prospects.

Biological interfacing of graphene and 2D materials in general has become essential for the sake of biocompatibility, dispersibility and selectivity of innovative hybrid nanomaterials which could be applied to the biotechnological and biomedical fields.[19–21] Chemical functionalization of 2D materials can imply noticeable drawbacks such as disrupture of the electronic structure.[22] To circumvent these drawbacks milder techniques of functionalization have been implemented. For instance, for graphene[23] and MoS_2,[24] recently interfaced with a biomolecule such as a protein, the functionalization process can be regarded as a biofunctionalization with the formation of a hybrid structure. Because of their wide range of functionalities and high responsiveness to a variety of stimuli, proteins are suitable candidates for bioconjugation of nanomaterials for quite a number of

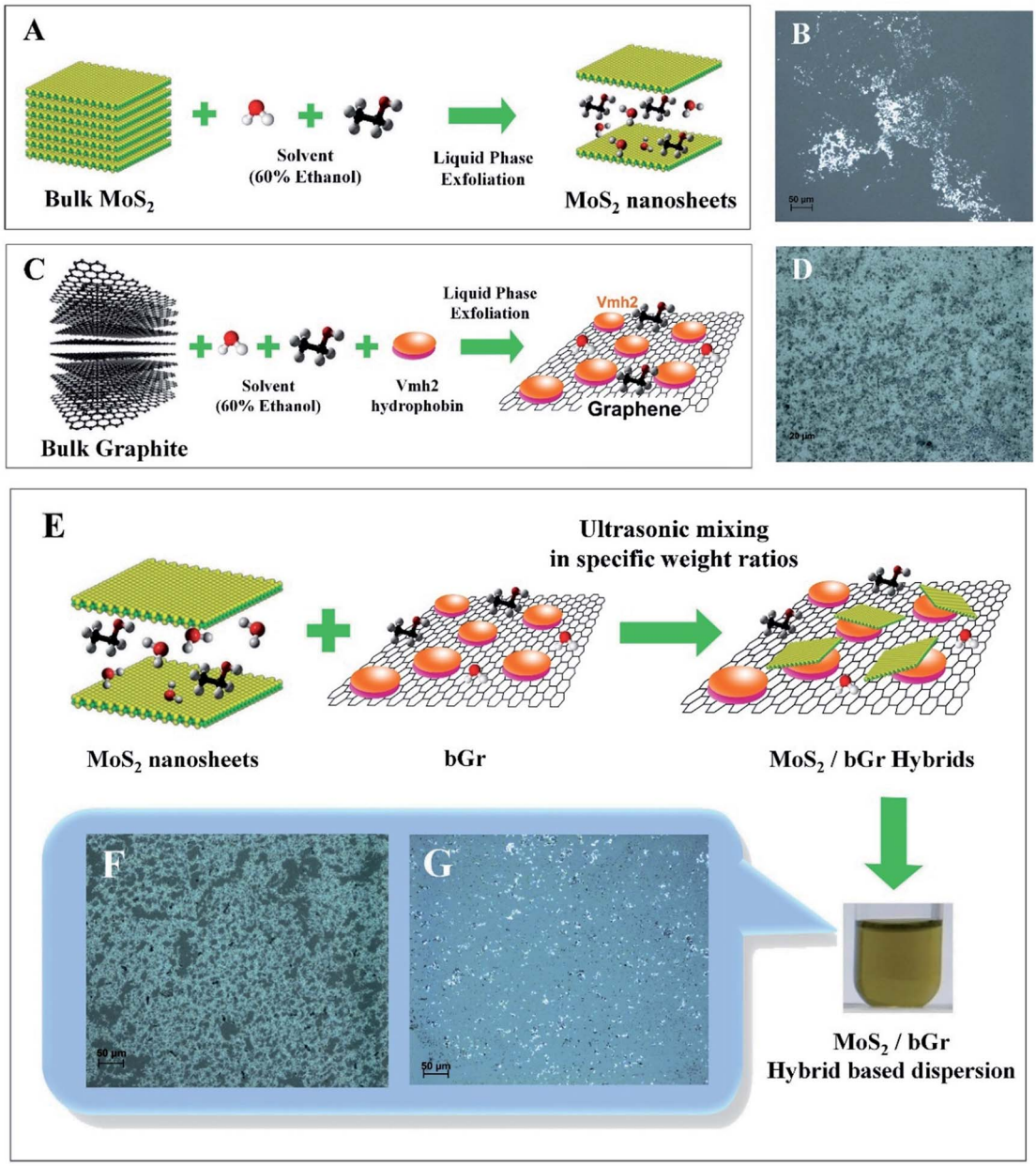

Fig. 1 Schematic diagram of production process for MoS_2/bGr hybrid structures. (A) Liquid phase exfoliation of MoS_2. (B) Reflected-light image of MoS_2 dispersion on glass substrate. (C) Liquid phase exfoliation and biofunctionalization of graphene. (D) Reflected-light image of bGr dispersion on glass substrate. (E) Production of MoS_2/bGr hybrid structures through green route. (F, G) Reflected-light images of MoS_2/bGr hybrid structures.

applications.[25] In this regard, green synthesis routes of exfoliation should be developed, *i.e.* exfoliation protocols based in aqueous and possibly eco-friendly solvents, to diminish the impact of nanomaterials in health and environmental issues.

Proteins known as the hydrophobins (HFBs) are amphiphilic and compact/globular proteins of around 3 nm, extracted from fungi, and endowed with peculiar self-assembling mechanisms, high surface activity and propensity to surface adhesion.[24,26] Their self-assembled (mono)layers can be used as functional coatings, for the non-covalent immobilization of proteins and nanomaterials, biofunctionalization and stabilization of liquid dispersions of 2D materials.[26–29] The class I HFBs, can self-assemble into amyloid-like structures that play relevant biological functions as chemically stable coatings, and therefore they are called functional amyloids.[30] Since it has been discovered that they can mask the fungal spores to the immune system they have attracted much interest for their use in the biomedical field.[31]

Herein, we produce few-layered, defect-free nanosheets of MoS_2, and biofunctionalized graphene (bGr), which are conjugated to a self-assembling protein, dispersed in aqueous solutions, through a green route, shown in Fig. 1(A–D). The protein used is the class I HFB Vmh2 extracted from the edible basidiomycete fungus, *Pleurotus ostreatus*, commonly known as the oyster mushroom.[32,33] This protein plays a crucial role in the stability of both the graphene and MoS_2 based dispersion in aqueous alcoholic medium.[34,35] In addition, its conjugation to the graphene generates a positive ζ-potential on the surface of nanosheets.[36] However, the exfoliated MoS_2 nanosheets in the absence of Vmh2 exhibit a negative ζ-potential.[24] Here, we take advantage of the oppositely charged surfaces of the nanosheets of MoS_2 and bGr as source of electrostatic attraction to lead to attachment between the two types of sheets, followed by vdW interactions between the 2D crystals.[37,38]

The hybrid structures are further characterized through optimal imaging, scanning electron microscopy, transmission electron microscopy, Raman and photoluminescence (PL) spectroscopy. Interestingly, this novel approach of green-route production of hybrid structures of MoS_2/graphene is reliable, reproducible, and offers low-cost technology for mass production of devices based on heterostructures of 2D materials. Moreover, in this combination of MoS_2/bGr heterostructure, it forms a semiconductor/metal interface, which is an outstanding platform for photonics and electronic devices, such as in p–n junction diodes and transistors.[11,12,32,33] Since in this structure, the Vmh2 protein is also sandwiched between the 2D layers, we name this complex structure as MoS_2/bGr hybrid structure, which can have promising applications in bioelectronics, biosensing, bioimaging and photonic devices.[9,15,39] In particular, we discuss the applications of MoS_2/bGr hybrid structure in biosensing and photodetection.[8,34]

Experimental

Production of MoS_2 and bGr dispersions using green route through LPE

MoS_2 powder (Aldrich, 69860, particle size ~6 μm, density 5.06 g mL^{-1}), was exfoliated in 60% ethanol aqueous solution (35 mg in 5 mL) using a tip sonicator (Bandelin Ultrasound SONOPULS HD3200, maximum power 200 W, working frequency 20 kHz, MS 72 probe, running at 10% amplitude) for 2 hours in cylindrical glass tubes (15 mm diameter, 10 cm height, rounded bottom). The temperature of the dispersion during the sonication was controlled in an ice-water bath.

Next, 5 mg of graphite powder (Aldrich, 332461, mesh number of grains +100, >75%, particle size ~300 μm) in 5 mL of 60% ethanol solution was exfoliated in the presence of Vmh2 (50 μg mL^{-1}), using a tip sonicator (Bandelin, HD3200, MS 72 probe, running at 10% amplitude) for 5 hours in cylindrical glass tubes and cooling in an ice-water bath. The extraction of Vmh2 from *P. ostreatus* mycelia was carried out as reported elsewhere (see the detailed method in ESI†).[23,24] Briefly, *P. ostreatus* mycelia were treated with 2% sodium dodecyl sulfate (SDS) in a boiling water bath. The residue was freeze-dried and treated with 100% trifluoroacetic acid (TFA) in a water bath sonicator. The supernatant was dried, and then lipids were extracted in a mixture of water–methanol–chloroform 2 : 2 : 1 v/v. The precipitate was again freeze-dried, treated with TFA, dried in a stream of air, and dissolved in 60% ethanol. To ensure the purity of the protein, the procedure for removal of non-protein contaminants is discussed in ESI† and the purity of the protein was tested by SDS gel electrophoresis, and its conformation by circular dichroism analysis as reported elsewhere.[31]

In Fig. 1, the schematic diagram of MoS_2/bGr production is described, in which Fig. 1(A and C) represents the protocol of liquid processing of bulk powders of MoS_2 and graphite, along with Vmh2 hydrophobin, by dispersing in the solvent of 60% ethanol, exfoliated through tip sonication, followed by step-wise controlled centrifugation. After sonication, dark dispersions of both MoS_2 and bGr samples were produced, consisting of heterogeneous number of layers. Both the dispersions of MoS_2 and bGr were centrifuged using step-wise controlled centrifugation (using Eppendorf Centrifuge 5810R, Rotor F-34-6-38) from 40*g* to 2400*g* for 45 minutes each step, for size selection and efficient production of monolayer enriched dispersions. The non-exfoliated crystallites were removed with low centrifugal force, 40*g* for 45 minutes, and the dispersion produced contains few-layered flakes with a wide distribution of size and thickness and a small percentage of monolayers population with varying lateral sizes.

The supernatant was then centrifuged with a higher force of 150*g* for 45 minutes and the pellets were removed. Further, the supernatant was separated and again centrifuged with a higher centrifugal force of 600*g* for 45 minutes and finally the associated supernatant was proceeded to the highest centrifugal force of 2400*g* for 45 minutes. The final dispersions of MoS_2 and bGr were drop-casted on the glass substrates for acquiring their morphological analysis through the optical microscope, detailed in ESI† with 50× objective.

Mixing of dispersions to produce MoS_2/bGr hybrid based solutions

After the preparation of bGr dispersion, we post-centrifuged the bGr dispersion for 45 minutes at 16 000*g* in a centrifuge

(Eppendorf Centrifuge 5415D) and separated the supernatant containing the excess of Vmh2 and 60% ethanol, and the bGr pellet was re-suspended in the MoS_2 solution in specific concentrations. Without removing the excess of hydrophobin in solution, the hybrid formation was not efficient, since excess of Vmh2 interacts with MoS_2 which acts as a hindrance for the interaction between layers of bGr and MoS_2. Thus, this step of post-centrifugation of bGr dispersion is somewhat tricky and crucial for the preparation of the MoS_2/bGr hybrid solution.

The produced dispersion of MoS_2 and bGr were mixed in various weight ratios of MoS_2 : bGr = 1 : 2, 1 : 4 and 1 : 10 to reach the optimal ratio in order to produce 2D hybrid solutions, and out of these 1 : 2 turned out to be the best weight ratio of MoS_2 : bGr, based on the formation of vdW heterostructures, as investigated further by SEM and Raman measurements. The scheme of preparation of the hybrid dispersion is shown in Fig. 1(E). Fig. 1(G) exhibits the optical image of the hybrid sample dried on the glass substrate with weight ratio of MoS_2 : bGr solutions corresponding to 1 : 2, whereas Fig. 1(F) shows the optical image of the hybrid sample with MoS_2 : bGr weight ratio corresponding to 1 : 10.

Characterizations

Optical extinction spectra were acquired of the dispersions of MoS_2 and bGr through UV-Vis spectrophotometer, experimental details are reported in ESI.† The surface morphology of few-layered nanosheets of MoS_2, bGr and MoS_2/bGr hybrids was characterized by optical microscopy, scanning electron microscopy (SEM) with EDS measurements and transmission electron microscopy (TEM), detailed in ESI.† Raman and PL spectroscopy were performed using a confocal Raman microscope with a laser line at 514 nm.

Results and discussion

The green route of production involves the liquid processing of bulk materials, which produces few-layered and high-quality MoS_2 and bGr samples. After the production of MoS_2 and bGr dispersions, the extinction spectra in the UV-Vis region of the MoS_2 and bGr samples were acquired after the final steps of centrifugation and analyzed. The extinction spectra of MoS_2 normalized at 350 nm after the final steps of centrifugation of 600*g* and 2400*g* are shown in Fig. 2 and bGr absorption spectrum is shown in ESI.† Through this spectral profile, we estimated the mean number of layers per flakes, the mean lateral size and the concentration of the MoS_2 nanosheets, based on the formulation,[24,35] as shown in Table 1.

For the graphene dispersion, the absorbance (Fig. S1†) per unit length (λ = 660 nm) is defined as a function of the produced graphene concentration, which is an important parameter in characterizing the graphene dispersion.[36] The absorption coefficient previously established by Lotya and coworkers, (ε = 1390 L g^{-1} m^{-1}) is related to the absorbance, through the Lambert–Beer law. Thus, the final concentration of the produced graphene dispersion after centrifugation of 2500*g* is estimated to be 54 μg mL^{-1}. The mean lateral size for bGr

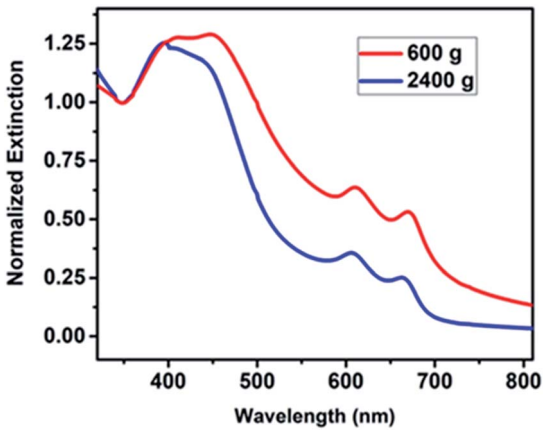

Fig. 2 Extinction spectra of MoS_2 normalized at 350 nm after centrifugation steps of 600*g* and 2400*g*.

Table 1 Mean number of layers per flake $\langle\bar{N}\rangle$, mean lateral size per flake $\langle\bar{L}\rangle$ and mean concentration of flakes $\langle\bar{C}\rangle$ in dispersion estimated by UV-Vis spectroscopy for liquid phase exfoliated MoS_2 after centrifugation at 2400*g*

Wavelength of A-exciton	$\langle\bar{N}\rangle$	$\langle\bar{L}\rangle$	$\langle\bar{C}\rangle$
662 nm	2.3 layers	100 nm	15.4 μg mL^{-1}

dispersion was previously estimated by Raman spectroscopy and reported by Gravagnuolo *et al.*[23] (mean number of layers, 2.9 ± 0.3 layers) after centrifugation at 2500*g*.

We also estimated the mean lateral size through dynamic light scattering (DLS), using the metrics reported by Lotya *et al.*[36,37] The lateral size was consistent among the UV-Vis and DLS metrics estimation for MoS_2 (Tables 1 and 2) and among the DLS metrics estimation and the mean lateral size for bGr previously reported (mean lateral size, 0.49 ± 0.06 μm after centrifugation at 2500*g*).[23] Since the lateral size of the protein is more than one order of magnitude smaller than that of the flakes, its presence on the surface cannot influence the analysis. Furthermore, ζ-potential of the flakes was obtained by electrophoretic mobility measurements of the centrifuged samples of MoS_2 and graphene. It was observed that after exfoliation, the flakes of bGr were positively charged; however the flakes of MoS_2 were negatively charged, as detailed in Table 2.

Thus, the oppositely charged flakes of MoS_2 and bGr become the source of interactions. The ζ-potential of the flakes of the

Table 2 ζ-Potential by Smoluchowski approximation and mean lateral size per flake $\langle\bar{L}\rangle$ estimated by electrophoretic mobility and Dynamic Light Scattering (DLS), for MoS_2, bGr and hybrid samples

	bGr	MoS_2	Hybrid
ζ-Potential (mV)	+35.4 ± 0.6	−22.5 ± 0.5	+24.5 ± 0.5
Mean lateral size and range (nm)	550 ± 40	125 ± 20	586 ± 58

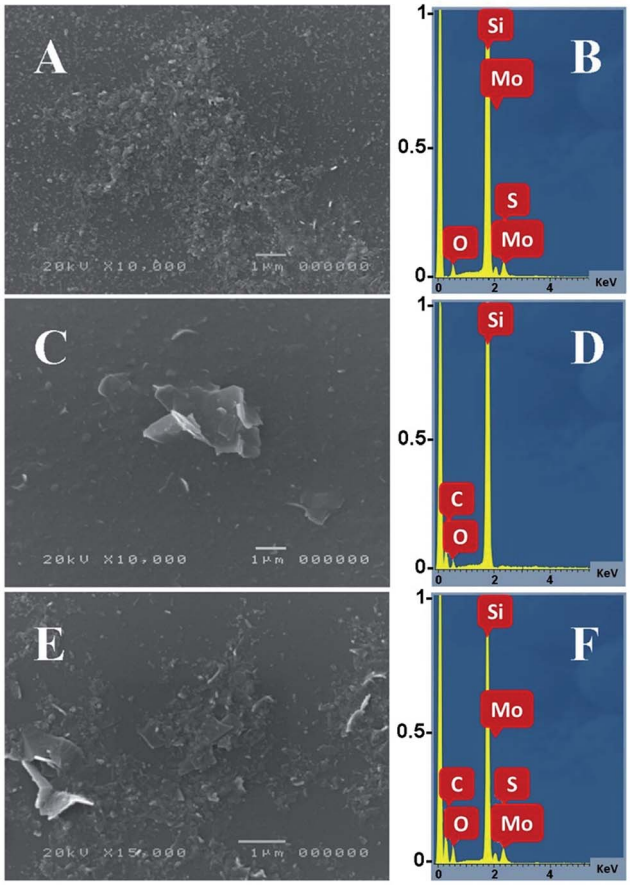

Fig. 3 SEM micrographs of MoS_2 (A), bGr (C) and hybrids (E) with their respective EDS measurements (B, D and F).

hybrid solution flakes were estimated in the range of +24 mV, which indicates the presence of Vmh2 hydrophobin in the hybrid dispersion, in between the layers of MoS_2 and graphene flakes. Moreover, with the addition of excess of Vmh2 (40–50 μL) to the prepared hybrid solution, the ζ-potential of the hybrid flakes has been observed to be enhanced by 10–12 mV, to achieve a higher stability over time for the hybrid dispersions.

The morphology of the films based on 2D materials was studied by using SEM.[23] Films were deposited onto SOI (silicon dioxide on silicon) substrates, shown in Fig. 3, with the relevant electron dispersive spectra (EDS) for the elemental analysis.[40] The few-layered solutions of 2D materials including MoS_2, bGr and the hybrid dispersions were drop-casted onto SOI substrate and dried in air. The samples were investigated initially without metallization for qualitative chemical analyses, after were metalized with gold by using a sputter coater, for morphological analyses and micrographs were acquired to 10 000× and 15 000× magnification. SEM micrographs confirmed that MoS_2 dispersion consists of nanosheets, with mean lateral size in the range of 100–150 nm, whereas bGr flakes were observed comparatively of bigger size, as shown in Fig. 3(A and C). The morphology of MoS_2/bGr hybrid sample is shown in Fig. 3(E), which consists of both the types of flakes, with bigger bGr nanosheets interfaced to and surrounded by smaller sized MoS_2 nanoflakes. The interfacial contact between the MoS_2 and bGr nanosheets is also observed in the hybrid sample through its SEM micrograph.

The EDS measurements were made for the elemental analysis, through which the presence of graphene in bGr, was represented by the carbon (C) peak and MoS_2 through molybdenum (Mo) and sulphur (S) peaks, shown in Fig. 3(B and D). Presence of the hydrophobin, Vmh2 also contributes to the C and O peaks. Moreover, in case of the hybrid sample, the peaks from all the elements Mo, S, C and O confirm the coexistence of MoS_2 and graphene (bGr) in the MoS_2/bGr hybrid structure, exhibited in Fig. 3(F). In addition, in all the spectra, there is presence of Si and O peaks from the silica glass substrate (SiO_2).

Fig. 4(A–C) show the TEM images of few-layered nanosheets of MoS_2 with higher resolution inset of MoS_2 nanoflakes, bGr nanosheets and MoS_2/bGr hybrids respectively. From TEM images, we confirm the size and morphology of MoS_2 nanosheets, the size lying in the 100 nm range, whereas for bGr flakes, the size is bigger, in the 500 nm range. Thus, TEM measurements are consistent with SEM results. Fig. 4(C) exhibits two different types of flakes of MoS_2 and bGr in contact with each other. The smaller nanosheets, MoS_2, lay on the surface of larger bGr flakes. Interestingly, no nanosheet is observed isolated from flakes, thus evidencing the strong affinity of MoS_2 nanosheet for bGr flakes due to their opposite polarity.

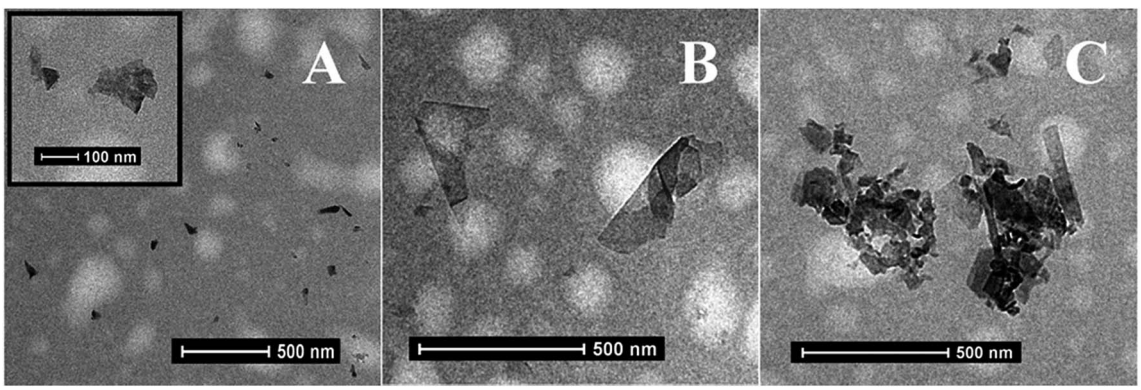

Fig. 4 TEM images of MoS_2 nanosheets (A) with higher resolution inset, bGr (B) and MoS_2/bGr hybrids (C).

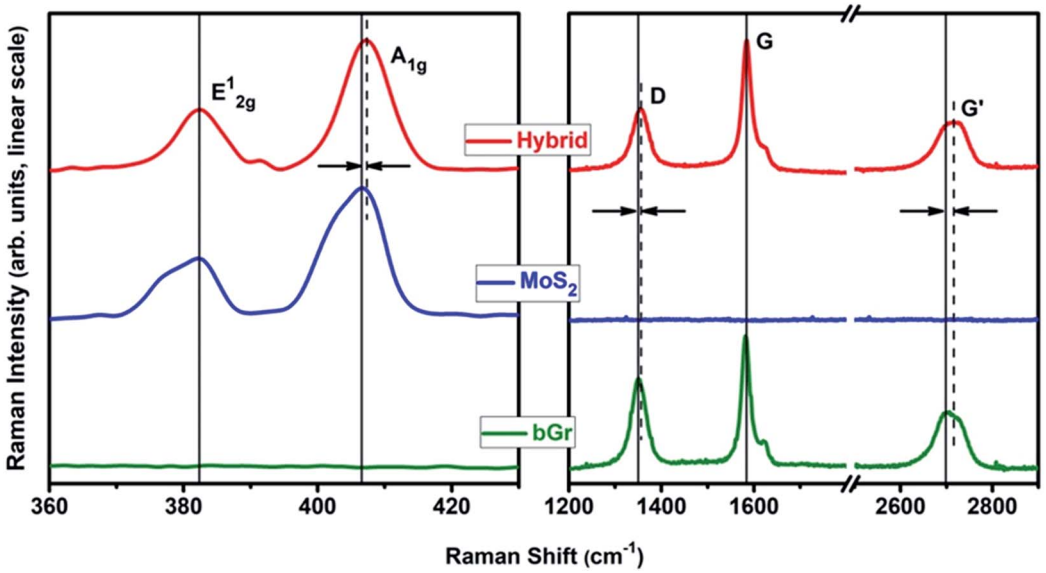

Fig. 5 Raman spectra of MoS_2, bGr and MoS_2/bGr hybrid samples (excitation wavelength of 514 nm, 4 mW at the sample).

The nanostructural and electronic properties of the exfoliated flakes of MoS_2, bGr and the produced hybrids, were investigated using Raman and PL spectroscopy at room temperature, which allows the determination of number of layers in MoS_2 and graphene. Moreover, Raman spectroscopy is a powerful tool to identify and quantify the quality of the MoS_2/bGr interface, to analyze the effect of the heterostructuring on the characteristic features of the parent homostructures of MoS_2 and graphene.[41–43] Raman spectra are particularly sensitive to materials nanostructuring, since nanoconfinement produces changes in several Raman features, including frequency, intensity and selection rules in most of the materials.[44–47] In addition, graphene and MoS_2 have been extensively studied, and correlation of Raman features and nanostructuring are reported elsewhere.[42–45,48]

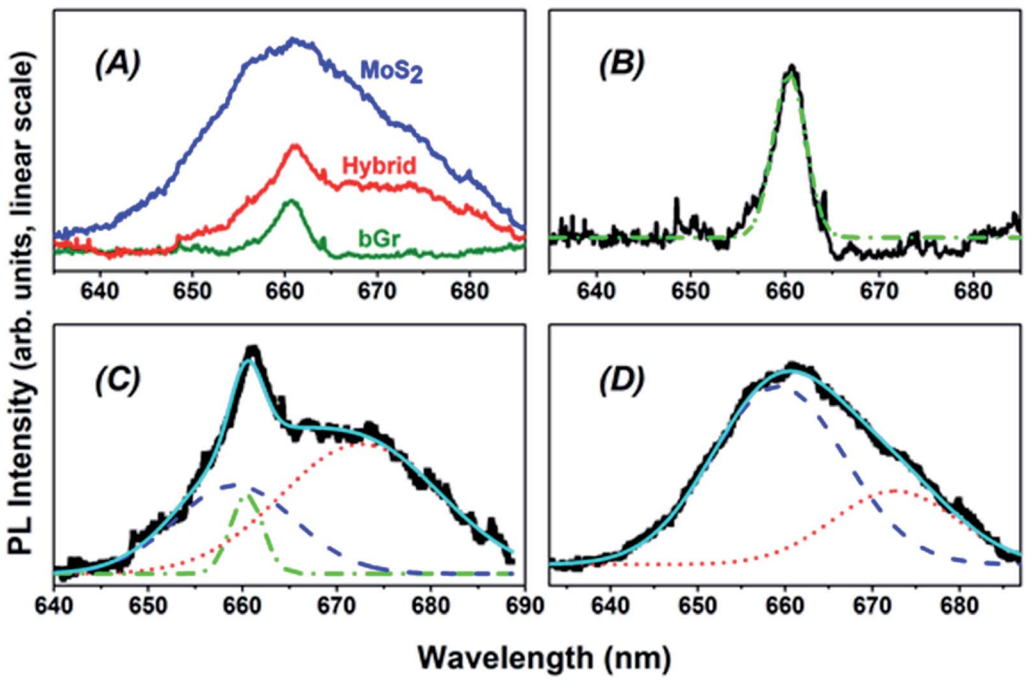

Fig. 6 (A) PL spectra of MoS_2, bGr and MoS_2/bGr hybrid samples (excitation wavelength 514 nm, 4 mW at the sample). (B) Gaussian best fit of bGr Raman signal at 4300 cm^{-1} (C) PL of MoS_2/bGr hybrid with Gaussian best fits of the bGr Raman peak (green, dash – dotted), exciton (A, blue dashed) and trion (A^-, red dotted) PL components by MoS_2 flakes. (D) PL spectra of MoS_2 flakes with Gaussian best fits for the exciton (A, blue dashed) and trion (A^-, red dotted) components of PL.

On excitation with wavelength of 514.5 nm, we collected the Raman spectra shown in Fig. 5. In the low frequency region, (Fig. 5) MoS_2 homostructures exhibit two major Raman bands (A_{1g} and E^1_{2g}) at 406.2 cm^{-1} and 382.7 cm^{-1}, respectively, which are significantly different from the starting bulk material.[48,49] The wavenumber differences between the A_{1g} and E^1_{2g} (23.5 cm^{-1}) is indicative of a nanostructuring corresponding to 3–4 layers.[24] Upon heterostructuring with graphene, the Raman-active phonon modes provide information on the interaction between the two crystals. In particular, the Raman features of MoS_2 are modified, with the out-of-plane mode, A_{1g} peak upshifts by 1.4 cm^{-1}, which gives the evidence for the quality of the interfacial contact, whereas E^1_{2g} is slightly upshifted by 0.5 cm^{-1}, which provides information about the in-plane strain. Furthermore, upon interfacing between the crystals, MoS_2 Raman peaks are comparatively broader than those of its hybrid (Fig. 5).

The Raman spectra of bGr exhibits a D band at 1350 cm^{-1} (1354 cm^{-1}, in MoS_2/bGr hybrid), a G band at 1582 cm^{-1} (invariant in the hybrid), and a G′ band at 2700 cm^{-1} (shifted to 2714 cm^{-1} in the hybrid). The ratio between the G and G′ band and the shape of the G′ band indicates a bi-layered graphene for the homostructure.[23] Thus, in case of MoS_2/bGr hybrid structure, the vdW contact is well characterized by the upshift of 14 cm^{-1} of the G′ band of graphene. Upon interfacing the MoS_2 and bGr sheets, the shape and symmetry of band changes, indicating a significant effect of vdW interactions and coupling between the layered materials.

Another significant evidence of electronic coupling between MoS_2 and bGr is also apparent from the PL measurements (Fig. 6(A–C)). Note worthily, upon excitation with 514.5 nm, graphene is not photoluminescent, and the band at 661 nm shown in Fig. 6(A) and in the inset of Fig. 6(C) corresponds to a multi-phonon Raman scattering peak of around 4300 cm^{-1},

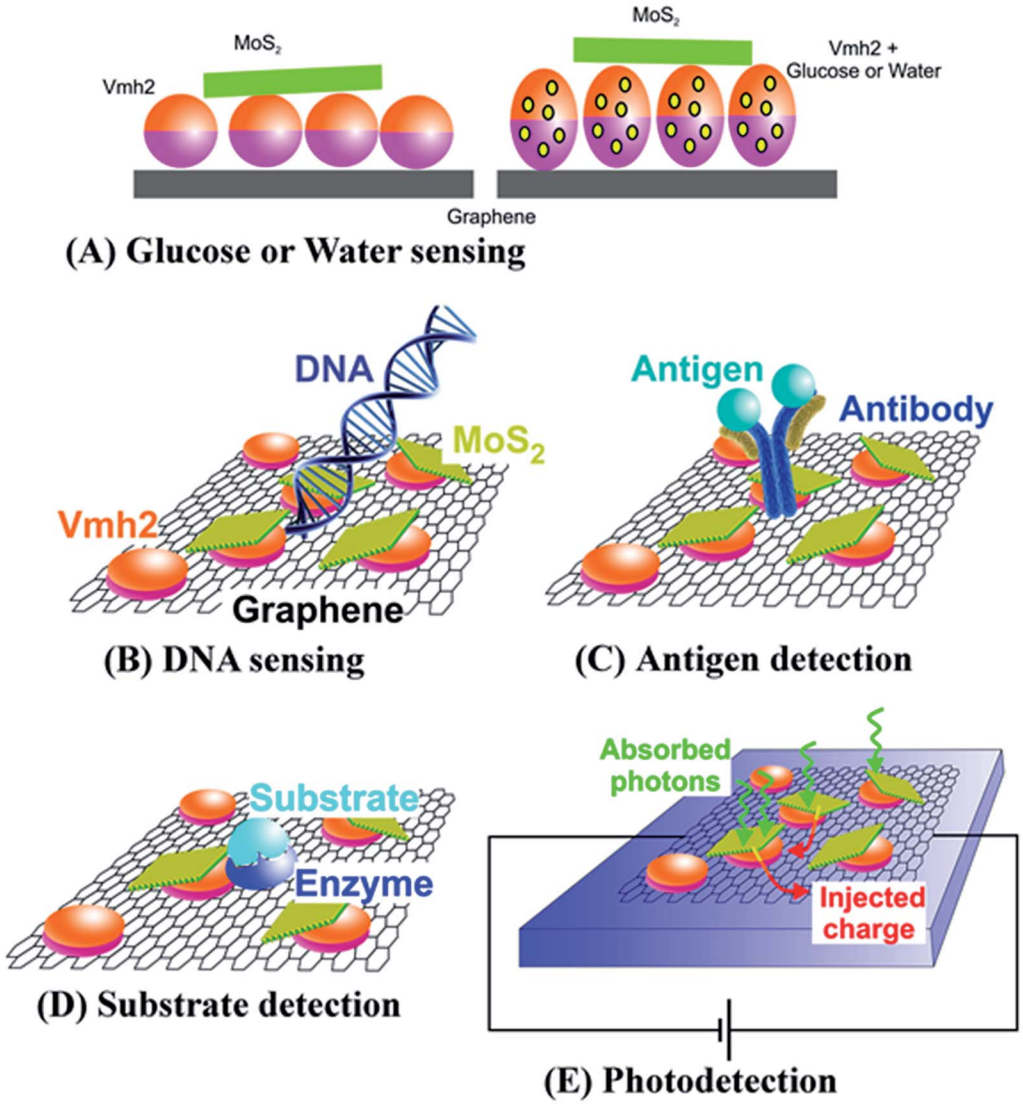

Fig. 7 Applications of MoS_2/bGr hybrid structure: (A) glucose or water molecules sensing, (B) DNA hybridization, (C) optical sensing *via* antibody–antigens complex, (D) optical sensing *via* enzyme–substrate complex, (E) photodetection mechanism.

present both in the graphene homostructure and in MoS_2/bGr hybrid when excited with 514.5 nm.[50] On the contrary, MoS_2 is photoluminescent, confirming the presence of monolayers in MoS_2 flakes, which is due to the change from indirect to direct bandgap.[51] In particular, in Fig. 6(B) we can identify the exciton (A) and trion (A^-) contributions to the emitted band, centered at 659 and 673 nm, respectively.[52] These correspond to the energy values of the emitted photon of 1.88 and 1.84 eV, respectively, in good agreement with previous measurement in MoS_2 flakes.[34]

In case of MoS_2/bGr hybrid (Fig. 6(C)), PL emission is strongly quenched (an overall <70%) due to the effect of interfacial charge transfer, between the layers of hybrids.[41,53] Modifications are also observed in the shape of PL spectra of the hybrid structure, when compared with the parent homostructures. In fact, our analysis based on Gaussian best fits of the A and A^- contributions points out that, while for the pure MoS_2 flakes the former peak contains a signal nearly three times larger than the latter, in the case of the hybrid this ratio gets $\approx$0.4, indicating a much stronger quenching of PL for the exciton. Concluding this remark, it can be certainly confirmed a strong electronic interaction and interlayer coupling between the layers of 2D crystals in the MoS_2/bGr hybrid structure.

In Fig. 7, we propose some applications of the MoS_2/bGr hybrid structures in biosensing and light sensing devices. It is well known that hydrophobin binds some molecules, like water[54] or glucose,[55] leading to the expansion of the interlayer space between the crystal layers of the hybrid, thus producing variation in the PL yield of MoS_2. Therefore MoS_2/bGr structure can be employed for water molecular sensing and glucose detection by exciting with an optical source. The principle of this application is shown in Fig. 7(A). Furthermore, as reported by Loan *et al.*,[34] MoS_2 and graphene are suitable components for the detection of specific DNA molecules, by exploiting PL quenching due to the presence of monolayered MoS_2 flakes in the graphene/MoS_2 heterostructure,[49] as sketched in Fig. 7(B).

Additionally, in our hybrid system, the presence of Vmh2 hydrophobin makes graphene a bio-functionalized material. This provides the hybrid a biocompatible interface and enables non-covalent conjugation with other proteins, such as antibodies and enzymes, as depicted in Fig. 7(C and D).[56,57] When attached to the MoS_2/bGr hybrid, these proteins can recognize and bind specific molecules, which changes the PL signal of monolayered MoS_2, thus providing a reliable optical method for biosensing applications.[9,58] In Fig. 7(E), we illustrate the use of MoS_2/bGr hybrid as a micro/nano photodetector. In this application, laser light would be efficiently absorbed by MoS_2, thus likely injecting free carriers in the biased conductive graphene layers, which could produce a measurable photocurrent on supplying external bias.[59,60]

Conclusions

In this work, we have produced dispersions of few-layered, defect-free and luminescent sheets of MoS_2, and bilayered biofunctionalized sheets of graphene with a self-assembling protein, *i.e.* the hydrophobin Vmh2, through the green route of scalable production. Vmh2 is adsorbed on the surface of the graphene sheets, which is used to tune the ζ-potential and the colloidal stability of the produced bGr dispersion. Then the nano-bio hybrid structures of MoS_2/bGr are produced by mixing of the dispersions (after removing the unbound Vmh2 by post-centrifugation and removing the supernatant), which are quite stable in liquid phase and can also be drop-casted on various substrates for making 2D heterostructure based films and coatings. Absorption measurements estimate the final concentration for dispersions of bGr and MoS_2, mean lateral size and mean thickness of the nanosheets of MoS_2. DLS measurements confirm the mean lateral size of the nanosheets. ζ-Potential analysis is performed to estimate the surface potential of the nanosheets, which is negative for MoS_2 and positive for bGr due to presence of Vmh2.

SEM and TEM imaging exhibits the morphology and texture of the 2D materials based films. Through Raman spectroscopy, the electronic properties of the exfoliated crystals of MoS_2 and bGr have been confirmed to that of the pristine materials. Moreover, significant modifications in the Raman features are observed in the MoS_2/bGr heterostructure sample, with respect to their homostructures. In particular, shifts are observed in the peak frequencies of MoS_2 in A_{1g} peak by +1.4 cm^{-1} and an upshift of 14 cm^{-1} is observed in G′ band of hybrids compared with bGr. These are the signatures of electronic interlayer coupling and strain effect produced between layers of 2D structures, which lead to formation of vdW heterostructures. PL emission confirms the presence of monolayers in MoS_2 flakes, which is quenched (>70%) due to the effect of interfacial charge transfer, between the layers of MoS_2/bGr hybrid materials. Also, changes are observed in the shape of PL spectra other than quenching effect. Multi-phonon Raman scattering peak of graphene around 4300 cm^{-1} is observed in the spectral range of MoS_2 PL emission.

Conclusively, we describe a green and scalable route of production of 2D materials based hybrid structures in which 2D materials layers are coupled by electrostatic vdW interactions. This technique of preparation of nanosheets is versatile, and can be easily extended to other 2D materials interfaced with various biomolecules for a wide range of applications from bioimaging and optoelectronics to optical biosensing. Moreover, this tool can be extended to the fabrication of innovative and application-specific nano-bio-hybrid systems with novel and tailored properties and multi-functionalities.

Conflicts of interest

There are no conflicts to declare.

Acknowledgements

The research was supported through the project IENA ("Immobilization of Enzymes on hydrophobin-functionalized NAnomaterials") within the framework of the University research program "Programma per il finanziamento della ricerca di Ateneo" D. R. n. 409 7/02/2017. The authors thank Dr Marinella Pirozzi of the Bioimaging Facility, Institute of Protein Biochemistry (CNR), Naples, for help with TEM experiments.

The authors are also obliged to Prof. Lorenzo Marrucci for his financial support and Mr Manjot Singh, PhD student, for his assistance in the experimental protocols, both based at the Department of Physics "Ettore Pancini", University of Naples "Federico II", Naples.

References

1 R. F. Service, *Science*, 2015, **348**, 490–492.
2 G. R. Bhimanapati, Z. Lin, V. Meunier, Y. Jung, J. Cha, S. Das, D. Xiao, Y. Son, M. S. Strano, V. R. Cooper, L. Liang, S. G. Louie, E. Ringe, W. Zhou, S. S. Kim, R. R. Naik, B. G. Sumpter, H. Terrones, F. Xia, Y. Wang, J. Zhu, D. Akinwande, N. Alem, J. A. Schuller, R. E. Schaak, M. Terrones and J. A. Robinson, *ACS Nano*, 2015, **9**, 11509–11539.
3 A. C. Ferrari, F. Bonaccorso, V. Fal'ko, K. S. Novoselov, S. Roche, P. Bøggild, S. Borini, F. H. L. Koppens, V. Palermo, N. Pugno, J. A. Garrido, R. Sordan, A. Bianco, L. Ballerini, M. Prato, E. Lidorikis, J. Kivioja, C. Marinelli, T. Ryhänen, A. Morpurgo, J. N. Coleman, V. Nicolosi, L. Colombo, A. Fert, M. Garcia-Hernandez, A. Bachtold, G. F. Schneider, F. Guinea, C. Dekker, M. Barbone, Z. Sun, C. Galiotis, A. N. Grigorenko, G. Konstantatos, A. Kis, M. Katsnelson, L. Vandersypen, A. Loiseau, V. Morandi, D. Neumaier, E. Treossi, V. Pellegrini, M. Polini, A. Tredicucci, G. M. Williams, B. Hee Hong, J.-H. Ahn, J. Min Kim, H. Zirath, B. J. van Wees, H. van der Zant, L. Occhipinti, A. Di Matteo, I. A. Kinloch, T. Seyller, E. Quesnel, X. Feng, K. Teo, N. Rupesinghe, P. Hakonen, S. R. T. Neil, Q. Tannock, T. Löfwander and J. Kinaret, *Nanoscale*, 2015, **7**, 4598–4810.
4 K. S. Novoselov, V. I. Fal′ko, L. Colombo, P. R. Gellert, M. G. Schwab and K. Kim, *Nature*, 2012, **490**, 192–200.
5 Z. Lin, A. McCreary, N. Briggs, S. Subramanian, K. Zhang, Y. Sun, X. Li, N. J. Borys, H. Yuan, S. K. Fullerton-Shirey, A. Chernikov, H. Zhao, S. McDonnell, A. M. Lindenberg, K. Xiao, B. J. LeRoy, M. Drndić, J. C. M. Hwang, J. Park, M. Chhowalla, R. E. Schaak, A. Javey, M. C. Hersam, J. Robinson and M. Terrones, *2D Mater.*, 2016, **3**, 42001.
6 L. Britnell, R. M. Ribeiro, A. Eckmann, R. Jalil, B. D. Belle, A. Mishchenko, Y. Kim, R. V Gorbachev, T. Georgiou, S. V Morozov, A. N. Grigorenko, A. K. Geim, C. Casiraghi, A. H. C. Neto and K. S. Novoselov, *Science*, 2013, **340**, 1311–1314.
7 T. Georgiou, R. Jalil, B. D. Belle, L. Britnell, R. V. Gorbachev, S. V. Morozov, Y.-J. Kim, A. Gholinia, S. J. Haigh, O. Makarovsky, L. Eaves, L. A. Ponomarenko, A. K. Geim, K. S. Novoselov and A. Mishchenko, *Nat. Nanotechnol.*, 2012, **8**, 100–103.
8 D. Jariwala, T. J. Marks and M. C. Hersam, *Nat. Mater.*, 2016, **16**, 170–181.
9 R. Kurapati, K. Kostarelos, M. Prato and A. Bianco, *Adv. Mater.*, 2016, **28**(29), 6052–6074.
10 W. Xia, L. Dai, P. Yu, X. Tong, W. Song, G. Zhang and Z. M. Wang, *Nanoscale*, 2017, **13**, 4324–4365.
11 D. Pierucci, H. Henck, J. Avila, A. Balan, C. Naylor, G. Patriarche, *et al.*, *Nano Lett.*, 2016, **16**, 4054–4061.
12 R. Liu, B. Liao, X. Guo, D. Hu, H. Hu, L. Du, H. Yu, G. Zhang, X. Yang and Q. Dai, *Nanoscale*, 2017, **9**, 208–215.
13 J. Shen, Y. He, J. Wu, C. Gao, K. Keyshar, X. Zhang, Y. Yang, M. Ye, R. Vajtai, J. Lou and P. M. Ajayan, *Nano Lett.*, 2015, **15**, 5449–5454.
14 J. Kang, V. K. Sangwan, J. D. Wood and M. C. Hersam, *Acc. Chem. Res.*, 2017, **50**, 943–951.
15 D. McManus, S. Vranic, F. Withers, V. Sanchez-Romaguera, M. Macucci, H. Yang, R. Sorrentino, K. Parvez, S.-K. Son, G. Iannaccone, K. Kostarelos, G. Fiori and C. Casiraghi, *Nat. Nanotechnol.*, 2017, **12**, 343–350.
16 J. Choi, H. Zhang, H. Du and J. H. Choi, *ACS Appl. Mater. Interfaces*, 2016, **8**, 8864–8869.
17 C. Backes, T. M. Higgins, A. Kelly, C. Boland, A. Harvey, D. Hanlon and J. N. Coleman, *Chem. Mater.*, 2017, **29**, 243–255.
18 A. Jawaid, D. Nepal, K. Park, M. Jespersen, A. Qualley, P. Mirau, L. F. Drummy and R. A. Vaia, *Chem. Mater.*, 2016, **28**, 337–348.
19 Y. Chen, C. Tan, H. Zhang and L. Wang, *Chem. Soc. Rev.*, 2015, **44**, 2681–2741.
20 P. Cicatiello, P. Dardano, M. Pirozzi, A. M. Gravagnuolo, L. De Stefano and P. Giardina, *Biotechnol. Bioeng.*, 2017, **9999**, 1–14.
21 K. Yang, Y. Li, X. Tan, R. Peng and Z. Liu, *Small*, 2013, **9**, 1492–1503.
22 T. S. Sreeprasad and V. Berry, *Small*, 2013, **9**, 341–350.
23 A. M. Gravagnuolo, E. Morales-Narváez, S. Longobardi, E. T. Da Silva, P. Giardina and A. Merkoçi, *Adv. Funct. Mater.*, 2015, **25**, 2771–2779.
24 J. Kaur, A. M. Gravagnuolo, P. Maddalena, C. Altucci, P. Giardina and F. Gesuele, *RSC Adv.*, 2017, **7**, 22400–22408.
25 M. Siepi, E. Morales-Narváez, N. Domingo, D. M. Monti, E. Notomista and A. Merkoçi, *2D Mater.*, 2017, **4**, 035007.
26 A. M. Gravagnuolo, E. Morales-Narváez, C. R. S. Matos, S. Longobardi, P. Giardina and A. Merkoçi, *Adv. Funct. Mat.*, 2015, **25**, 6084–6092.
27 P. Laaksonen, M. Kainlauri, T. Laaksonen, A. Shchepetov, H. Jiang, J. Ahopelto and M. B. Linder, *Angew. Chem., Int. Ed.*, 2010, **49**, 4946–4949.
28 V. Aimanianda, J. Bayry, S. Bozza, O. Kniemeyer, K. Perruccio, S. R. Elluru, C. Clavaud, S. Paris, A. A. Brakhage, S. V. Kaveri, L. Romani and J. P. Latgé, *Nature*, 2009, **460**, 1117–1121.
29 A. M. Gravagnuolo, S. Longobardi, A. Luchini, M. S. Appavou, L. De Stefano, E. Notomista, L. Paduano and P. Giardina, *Biomacromolecules*, 2016, **17**, 954–964.
30 D. L. Cheung, *Langmuir*, 2012, **28**, 8730–8736.
31 S. Longobardi, D. Picone, C. Ercole, R. Spadaccini, L. De Stefano, I. Rea and P. Giardina, *Biomacromolecules*, 2012, **13**, 743–750.
32 J. Y. Kwak, J. Hwang, B. Calderon, H. Alsalman, N. Munoz, B. Schutter and M. G. Spencer, *Nano Lett.*, 2014, **14**, 4511–4516.

33 S. Rathi, I. Lee, D. Lim, J. Wang, Y. Ochiai and N. Aoki, *Nano Lett.*, 2015, **15**, 5017–5024.
34 P. T. K. Loan, W. Zhang, C. T. Lin, K. H. Wei, L. J. Li and C. H. Chen, *Adv. Mater.*, 2014, **26**, 4838–4844.
35 C. Backes, R. J. Smith, N. Mcevoy, N. C. Berner, D. Mccloskey, H. C. Nerl, A. O. Neill, P. J. King, T. Higgins, D. Hanlon, N. Scheuschner, J. Maultzsch, L. Houben, G. S. Duesberg, J. F. Donegan, V. Nicolosi and J. N. Coleman, *Nat. Commun.*, 2014, **5**, 4576.
36 M. Lotya, Y. Hernandez, P. J. King, R. J. Smith, V. Nicolosi, L. S. Karlsson, F. M. Blighe, S. De, W. Zhiming, I. T. McGovern, G. S. Duesberg and J. N. Coleman, *J. Am. Chem. Soc.*, 2009, **131**, 3611–3620.
37 M. Lotya, A. Rakovich, J. F. Donegan and J. N. Coleman, *Nanotechnology*, 2013, **24**, 265703–265709.
38 K. Zhou, F. Withers, Y. Cao, S. Hu, G. Yu and C. Casiraghi, *ACS Nano*, 2014, **8**, 9914–9924.
39 Q. Liu, B. Cook, M. Gong, Y. Gong, D. Ewing, M. Casper, A. Stramel and J. Wu, *ACS Appl. Mater. Interfaces*, 2017, **9**, 12728–12733.
40 K. Singh, S. Kumar, K. Agarwal, K. Soni, V. R. Gedela and K. Ghosh, *Sci. Rep.*, 2017, **7**, 1–12.
41 A. C. Ferrari, J. C. Meyer, V. Scardaci, C. Casiraghi, M. Lazzeri, S. Piscanec, K. S. Novoselov, S. Roth and A. K. Geim, *Phys. Rev. Lett.*, 2006, **97**, 187401.
42 H. Li, Q. Zhang, C. C. R. Yap, B. K. Tay, T. H. T. Edwin, A. Olivier and D. Baillargeat, *Adv. Funct. Mater.*, 2012, **22**, 1385–1390.
43 L. Sirleto, A. Vergara and M. A. Ferrara, *Adv. Opt. Photonics*, 2017, **9**, 169.
44 A. Jorio, R. Saito, G. Dresselhaus and M. S. Dresselhaus, *Raman Spectroscopy in Graphene Related Systems*, 2011.
45 M. Alfè, V. Gargiulo, R. Di Capua, F. Chiarella, J.-N. Rouzaud, A. Vergara and A. Ciajolo, *ACS Appl. Mater. Interfaces*, 2012, **4**, 4491–4498.
46 U. Coscia, G. Ambrosone, F. Gesuele, V. Grossi, V. Parisi, S. Schutzmann and D. K. Basa, *Appl. Surf. Sci.*, 2007, **254**(4), 984–988.
47 J. Kaur, J. Shah, R. K. Kotnala and K. C. Verma, *Ceram. Int.*, 2012, **38**(7), 5563–5570.
48 C. Lee, H. Yan, L. Brus, T. Heinz, J. Hone and S. Ryu, *ACS Nano*, 2010, **4**, 2695–2700.
49 X. Zhang, X. Qiao, W. Shi, J. Wu, D. Jiang and P. Tan, *Chem. Soc. Rev.*, 2015, **44**, 2757–2785.
50 A. Splendiani, L. Sun, Y. Zhang, T. Li, J. Kim, C. Chim, G. Galli and F. Wang, *Nano Lett.*, 2010, **10**, 1271–1275.
51 K. F. Mak, C. Lee, J. Hone, J. Shan and T. Heinz, *Phys. Rev. Lett.*, 2010, **105**, 136805.
52 K. F. Mak, K. He, C. Lee, G. H. Lee, J. Hone, T. F. Heinz and J. Shan, *Nat. Mater.*, 2013, **12**, 207–211.
53 D. Pierucci, H. Henck, C. H. Naylor, H. Sediri, E. Lhuillier, A. Balan, J. E. Rault, Y. J. Dappe, F. Bertran, P. Le Fèvre, A. T. C. Johnson and A. Ouerghi, *Sci. Rep.*, 2016, **6**, 26656.
54 J. Tao, Y. Wang, Y. Xiao, P. Yao, C. Chen, W. Pang, H. Yang, D. Sun, Z. Wang and L. Jing, *Carbon N. Y.*, 2017, **116**, 695–702.
55 B. Della Ventura, I. Rea, A. Caliò, P. Giardina, A. M. Gravagnuolo, R. Funari, C. Altucci, R. Velotta and L. De Stefano, *Appl. Surf. Sci.*, 2016, **364**, 201–207.
56 L. De Stefano, I. Rea, E. De Tommasi, I. Rendina, L. Rotiroti, M. Giocondo, S. Longobardi, A. Armenante and P. Giardina, *Eur. Phys. J. E*, 2009, **30**, 181–185.
57 S. Longobardi, A. M. Gravagnuolo, I. Rea, L. De Stefano, G. Marino and P. Giardina, *Anal. Biochem.*, 2014, **449**, 9–16.
58 I. Song, C. Park and H. C. Choi, *RSC Adv.*, 2015, **5**, 7495–7514.
59 H. Xu, J. Wu, Q. Feng, N. Mao, C. Wang and J. Zhang, *Small*, 2014, **10**, 2300–2306.
60 Z. Huang, W. Han, T. Hongli, R. Long, C. D. Sathish, X. Qi and H. Zhang, *2D Mater.*, 2015, **2**, 35011.